IET Science, Measurement & Technology

WILEY

The Institution of Engineering and Technology

ORIGINAL RESEARCH OPEN ACCESS

Influence of Applied Voltage Waveforms on Ozone Generation and Operating Condition Optimisation in Surface DBD Reactors

Brahim el Khalil Oulad Naoui[1] | Said nemmich[1] | Kamel Nassour[2] | Essama Ahmed Ghaitaoui[2] | Amar Tilmatine[1] | Sherif Salama Mohamed Ghoneim[3] | Amanuel Kumsa Bojer[4] | Sayed Ahmed Nagy[5,6] | Ahmed Mohammed Attiya Soliman[5,6] | Ahmed M. Hussein[5,7]

[1]Laboratory the Applications of Plasma, Electrostatics and Electromagnetic Compatibility (APELEC), Djillali Liabes University of Sidi Bel-Abbes, Sidi Bel-Abbes, Algeria | [2]Intelligent Control & Electrical Power Systems Laboratory (ICEPS), Djillali Liabes University of Sidi Bel-Abbes, Sidi Bel-Abbes, Algeria | [3]Department of Electrical Engineering, College of Engineering, Taif University, Taif, Saudi Arabia | [4]Ethiopian Artificial Intelligence Institute, Addis Ababa, Ethiopia | [5]Department of Electrical Engineering, College of Engineering, University of Bisha, Bisha, Saudi Arabia | [6]Department of Electrical Engineering, Faculty of Engineering, Al-Azhar University, Cairo, Egypt | [7]Department of Electrical Engineering, Faculty of Engineering at Shubra, Benha University, Khalafawi, Cairo, Egypt

Correspondence: Amanuel Kumsa Bojer (amanuel.kumsa@aau.edu.et)

Received: 15 November 2025 | **Revised:** 24 March 2026 | **Accepted:** 24 April 2026

ABSTRACT

Surface dielectric barrier discharge (SDBD) ozone generators are a promising technology for industrial water treatment as well as air purification; however, they are under-studied. In this experimental study, three types of AC voltage waveforms (triangular, rectangular and sinusoidal) are compared to ozone generation and energy performance in the SDBD reactor. The optimal waveform was triangular, with an ozone concentration of 12 mg/L and an efficiency of 120 g/kWh. The second was the sinusoidal waveform (120 mg/L and 95 g/kWh, respectively). The most typical was the square waveform, with the rectangular one less effective. The optimum operating conditions are as follows (by response surface methodology (RSM)): $V = 7.84$ kV, $f = 202.86$ Hz ($\eta = 114.76$ g/kWh) and $V = 8.99$ kV, $f = 849.7$ Hz (OC = 132.163 mg/L). This study highlights the importance of optimal waveform selection and systematic parameter tuning to improve ozone generation performance while minimising energy consumption for practical industrial SDBD applications.

1 | Introduction

Ozone (0_3) consists of three atoms which are oxygen in nature. It has attracted great attention in the past because it can be utilised in various applications such as water purification, food preservation and air cleaning [1, 2]. The O_3 oxidising ability also makes it beneficial in medicine, as it can heal wounds and fight off infection because it is lethal to such a versatile group of bacteria [3–5]. It is one of the best methods to produce high-concentration ozone because it functions so efficiently [6, 7].

In the Dielectric Barrier Discharge (DBD) method, non-thermal plasma micro-discharges are formed in the region existing between two electrodes, at least one of them having a dielectric coating. These micro-discharges contribute to breaking down oxygen molecules (O_2), and the remaining oxygen atoms recombine to form ozone (O_3) [8, 9]. There are many different kinds of DBD reactors, but Volume Dielectric Barrier Discharge (VDBD) and Surface Dielectric Barrier Discharge (SDBD) are most commonly used [10, 11]. VDBD reactors are widely used, but SDBD reactors are superior in terms of energy efficiency and size, as evidenced by various recent studies [12].

This is an open access article under the terms of the Creative Commons Attribution-NonCommercial License, which permits use, distribution and reproduction in any medium, provided the original work is properly cited and is not used for commercial purposes.

© 2026 The Author(s). *IET Science, Measurement & Technology* published by John Wiley & Sons Ltd on behalf of The Institution of Engineering and Technology.

Pekarek et al. 2012 [13], investigated how the sinusoidal driving voltage and frequency affected ozone production in a radial SDBD reactor. Their study showed that the more ozone they make, the more discharge power they need, so these things are very important for making SDBD better for making people's ozone. K. Nassour et al. 2015 [7] conducted a comparative experimental study between small-scale VDBD and SDBD cylindrical ozone generators under the same experimental conditions. Their results demonstrated that although volume DBD reactors are predominantly used in industrial ozone generation, SDBD reactors exhibited significant superiority in terms of both ozone generation and energy efficiency compared to VDBD reactors. S. Xie et al. 2019 [14] employed a planar multi-electrode SDBD reactor with pure O_2 to find how to do ozone. They learnt that evening out the distribution of gas in the chamber dramatically boosted ozone production. Nemmich et al. 2019 [15] have previously shown the importance of obtaining an appropriate waveform for efficient ozone formation in a VDBD reactor and that distorted voltages on other shapes than sinusoidal or pulsed can have a significant effect on energy yield. B.Choudhury 2022 [16] investigated the ozone flow from a fan-shaped SDBD reactor and noticed that this configuration of electrodes allows ozone scatter to spread significantly better and thus accelerates decontamination compared with the conventional comb-shaped arrangement. Research is continuing on DBD technology aiming at increased energy efficiency based in part on better dielectric materials, optimal shaping of electrodes and further refinement of regulation of voltage waveforms. Also, scientists are exploring new reactor designs that can produce more ozone [17, 18].

Response surface methodology has also been successfully used to optimise the operating conditions for ozone generation. For instance, Nemmich et al. 2021 [19] developed an ozone food preservation system using RSM. This illustrates how this technique may identify the optimal conditions for increasing food shelf life in combination with the least possible energy. Nemmich et al. (2024) [20] also studied the ozone half-life generated by dielectric barrier discharge and demonstrated how effective RSM is to investigate and enhance the factors determining ozone generation. Although SDBD reactors have demonstrated clear superiority in terms of energy efficiency and ozone generation, research activity in this area remains limited compared to VDBD systems. This can be attributed to the fact that VDBD technology preceded SDBD by several years and became widely adopted across various industrial applications. As with any emerging technology, SDBD reactors require time to gain the confidence of the research community, despite their evident advantages. Consequently, systematic studies on SDBD reactors have not yet received the attention they deserve. Motivated by this observation, the present work investigates an important aspect that directly influences ozone generation efficiency in such reactors, namely the effect of applied voltage waveform shape.

This study has two main objectives. First, even though SDBD reactors have been shown to be better in many ways, there hasn't been a systematic comparison of how different voltage waveform shapes (triangular, rectangular, and sinusoidal) affect ozone generation and energy efficiency in SDBD systems. This study experimentally examines the impact of these three waveforms on the performance of the SDBD reactor. Second, there hasn't been enough research on how to use Response Surface Methodology (RSM) to improve SDBD operating conditions. This study uses RSM to find the best voltage and frequency settings for SDBD reactors in industrial settings, with the goal of finding the best operating conditions for making a lot of ozone while using as little energy as possible.

2 | Materials and Methods

2.1 | Ozone Generator

For this study, a SDBD ozone-generating system, as seen in Figure 1, is utilised. The axial symmetry for the proposed reactor follows a cylindrical coaxial anode-cathode configuration. A glass dielectric tube is placed between two metal electrodes of opposite polarity and serves as the primary insulating barrier therebetween. The tube dielectric is of glass, and due to mechanical constraints has a 'sweet' spot (radial wall thickness 2 mm) in order to force an efficient enough dielectric strength without losing too much axial length, necessary for discharge activation: (*length = 240 mm).

The high-voltage electrode, which is powered by the AC power source, consists of a cylindrical sleeve made from aluminium foil that is 140 mm long. This aluminium foil electrode is adhered closely to the inside wall of the glass tube so as to ensure a uniform electric field within the discharge space and a strong electrical connection therebetween, leading to fewer voltage drops and hot spots. The ground electrode assembly, which closes the electrical circuit, is made of 1 mm thick stainless-steel mesh. This mesh has a regular square grid design with openings in each cell that are 0.75 mm^2 in area. This lets gas pass through while keeping the electrical connection. The mesh electrode is inside and supported by a cylindrical stainless-steel housing with an internal diameter of 52 mm. This housing also serves as the wall of the reactor chamber. Because of this specific shape and choice of materials, the dielectric barrier discharge plasma starts and stays along the interface where the glass dielectric tube's outer surface touches the inner mesh electrode surface. This creates small micro-discharges that help the processes of oxygen dissociation and ozone formation.

2.2 | Experimental Set-Up

Figure 2 shows the experimental setup, which was made to evaluate how different voltage waveform shapes affect the SDBD reactor's energy efficiency and ozone concentration. It has all the parts it needs, like the reactor, the power supply system, and the measurement equipment, so that it can accurately measure the amount of ozone created under different electrical conditions and make precise changes to the voltage applied.

The ozone generator gets its power from a high-voltage (HV) amplifier (Trek, ±30 kV), and the function generator (Toellener Toe 7301) controls the shape of the waveform that goes to the power amplifier. The power amplifier can make voltage signals with triangular, rectangular, or sinusoidal waveforms. Its output voltage can be anywhere from 0 to ±30 kV DC or AC RMS, and its frequency can be anywhere from 0 to 3 kHz. We can change the RMS value of the voltage and the frequency separately.

17518830, 2026, 1, Downloaded from https://ietresearch.onlinelibrary.wiley.com/doi/10.1049/smt2.70070 by Egyptian National Sti. Network (Enstinet), Wiley Online Library on [24/06/2026]. See the Terms and Conditions (https://onlinelibrary.wiley.com/terms-and-conditions) on Wiley Online Library for rules of use; OA articles are governed by the applicable Creative Commons License

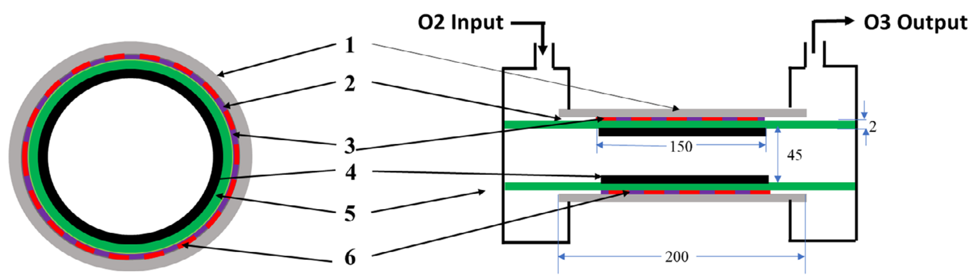

FIGURE 1 | Surface Dielectric Barrier Discharge reactor (SDBD). [20] 1. Grounded electrode, 2. Discharge gap, 3. Stainless-steel mesh, 4. HV electrode, 5. Glass tube and 6. Plasma.

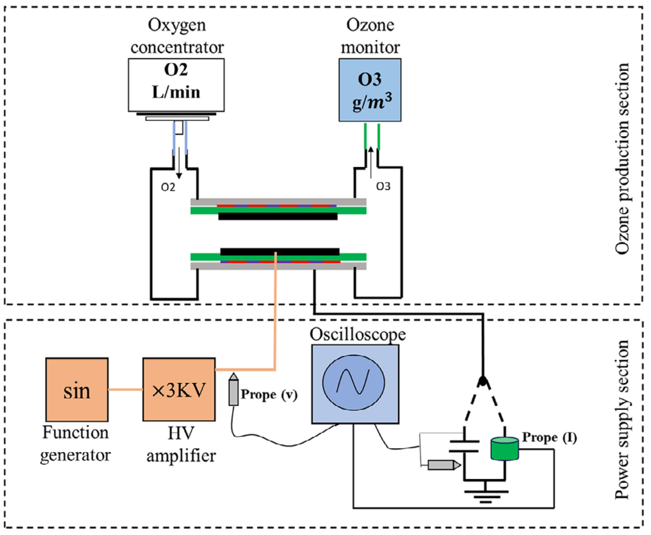

FIGURE 2 | Simplified schematic of the experimental setup.

The feed gas source for the ozone generator was an oxygen concentrator (NIDEK Medical Nuvo Lite Mark 5). This device produces a continuous flow of high-purity oxygen, which the DBD reactor needs to create ozone continuously. The concentrator is able to adjust oxygen flow from 0 to 10 L/min so that you can regulate the gas input precisely as required for your experiment. In this study, the flow rate of oxygen was 1 L/min to ensure that the time for an O_2 molecule staying in the gas phase between two electrodes was appropriate and that increasing ozone generation rate with reaction temperature were constant.

The ozone concentration produced by the reactor is measured continuously using an ozone monitor (Ozone Solutions, Model 106-H). This instrument allows for real-time measurement of the ozone concentration in the gas stream exiting the reactor. This is achieved through ultraviolet (UV) radiation absorption at 254 nm, which corresponds to the absorption maximum of the ozone molecule. The ozone concentration value is read directly from the analyser display and subsequently used to evaluate the performance of the ozone generator and assess the influence of the applied voltage waveforms on ozone production.

The voltage (RMS) and frequency can be adjusted separately. This flexibility is also desired for the possibility to assess the impact of each aspect separately. An applied voltage (V) is sensed with a high-voltage probe (Tektronix P6015 A), and the current is monitored using a high-frequency current sensor (Pearson Software Tools, current monitor 410, 20 MHz). The voltage and current readings are acquired in two channels of a digital oscilloscope (GWINSTEK GDS-3154).

The capacity was adopted to indirectly measure transferred charge to estimate the electrical characteristics of the discharge. The grounded electrode and the measuring circuit were connected in series with a reference capacitor (22 nF of capacity). The voltage drop across the capacitor can be used to determine the charge induced each discharge cycle with this configuration.

We then created a Lissajous figure to determine an estimate of the power used by the dielectric barrier discharge system. The Y-axis was the voltage (V), and the X-axis was the charge (q). This figure expresses in the interior how much energy it is lost per cycle. To get the average discharge power, multiply that by the operating frequency. This graphical approach is certainly a reliable and well-known way to analyse the energy in DBD reactors because it allows you to analyse the discharge process qualitatively as well as quantitatively [21].

A Lissajous representation can be used to figure out how much power the ozone generator uses with the three different voltage forms. The Lissajous area is equal to energy w(j) as in Equation 1.

$$W = \oint V.C.dv_c = \oint V.dq \tag{1}$$

where V is the applied voltage (V) and q is the transferred charge (C). The enclosed area of the Lissajous figure represents the energy W, which is then multiplied by the frequency f to calculate the discharge power P (W) [22].

$$P = W \times f \tag{2}$$

Finally, the energy efficiency was calculated using the following equation:

$$\eta = \frac{Y}{P} \tag{3}$$

where Y (g/h) represents the ozone generation, and P (kW) denotes the power consumed.

17518830, 2026, 1, Downloaded from https://ietresearch.onlinelibrary.wiley.com/doi/10.1049/smt2.70070 by Egyptian National Sti. Network (Enstinet), Wiley Online Library on [24/06/2026]. See the Terms and Conditions (https://onlinelibrary.wiley.com/terms-and-conditions) on Wiley Online Library for rules of use; OA articles are governed by the applicable Creative Commons License

3 | Experimental Designs Methodology

The methodology of experimental designs aids in ascertaining the requisite number of experiments to be executed in alignment with a clearly delineated objective. Examine the influence of diverse factors, reduce measurement variability, investigate the effects of factor interactions, and evaluate the distinct impact of factors and their interactions [23, 24].

Before starting the experimental investigations, it is very important to choose the right experimental design that can accurately mimic the process. This study employed the Composite Centred Faces (CCF) design framework, which enables the creation of a second-order multiple linear regression model. This design method makes it possible to find and describe the quadratic relationship that exists between the input variables u_i (where i = 1,. . . ,k), which are the independent factors, and the output function that is being optimised, which is called the response variable. Because this relationship is quadratic, it is possible to look at both linear and non-linear impacts in depth, as well as how the different elements interact with each other to affect the system's performance.

$$y = f\ (u_i) = c_0 + \sum c_i u_i + \sum c_{ij} u_i u_j + \sum c_{ii} {u_i}^2 \qquad (4)$$

With Δu_i and u_{i0} representing the variation increment and the central point of factor i, respectively, the normalized cantered values of the input factors can be calculated through the following mathematical expression:

$$x_i = (u_i - u_{i0})\,/\Delta u_i \qquad (5)$$

Using these additional variables, the output function turns into:

$$y = f\ (x_i) = a_0 + \sum a_i x_i + \sum a_{ij} x_i x_j + \sum a_{ii} {x_i}^2 \qquad (6)$$

In order to minimise the difference between the experimental results and the predicted mathematical model, a data processing program is used to compute or estimate coefficients [25].

MODDE 5.0 was the software used. It is a Windows program for developing and testing experiments [MODDE 5.0, 1999]. The software aids the user in deducing answers and understanding the results. It figures out the coefficients of the mathematical model and the best approach to change the variables to get the most out of the process. The program also figures out R^2 and Q^2, which are two important statistical measures that determine if the mathematical model is good or bad. R^2, or the goodness of fit, is a number that tells you how well the model matches the raw data. It goes from 0 to 1, where 0 means there is no model and 1 means the model is perfect. Q^2, which is also called goodness of prediction, tells us how effectively the model can guess what will happen in the future. The lowest point is minus infinity, and the highest point is 1. For a model to pass the diagnostic test, both parameters must be high and not more than 0.2–0.3 apart [26, 27].

4 | Results and Discussions

4.1 | Electrical Characterisation

An ozone generator that uses Surface Dielectric Barrier Discharge (SDBD) technology can be thought of as an electrical circuit that is made up of a capacitor and a resistor connected in series. Most people think of this setup as a capacitive load. In these operating conditions, the total current recorded during discharge is made up of two different parts: the micro-discharge current, which comes from localised plasma filaments, and the capacitive current, which comes from the dielectric barrier charging and discharging [28]. You can write these two current parts mathematically like this:

$$i\ (t) = C\frac{dV}{dt} \qquad (7)$$

where V and C represent the voltage and capacitance of the DBD reactor, respectively [29].

Figure 3 shows the voltage waveforms that were sent to the reactor and the corresponding discharge currents for triangular, rectangular and sinusoidal voltage waveforms. In a preliminary experiment, the applied voltage was gradually increased step by step from 3 kV to 9 kV until a homogeneous and stable discharge current was obtained in terms of discharge density. Based on these observations, 7.5 kV was selected as the reference voltage level, as it yielded the most stable and uniform discharge density across all three voltage waveforms. To avoid presenting a separate figure for each preliminary experiment, only the results obtained at 7.5 kV at a frequency of 500 Hz are presented in Figure 3, ensuring a clear and representative comparison between the three waveforms.

The present waveforms show two different groups of pulses in each cycle. During the positive half-cycle of the voltage, the discharges are denser and more stable, with peak discharge currents reaching about 120 mA. This is linked to the growth of positive streamers. On the other hand, the negative half-cycle is made up of micro-glow discharges, which happen less often and last for less time than the positive half-cycle [30, 31].

During the positive half-cycle, free electrons are pushed towards the anode, which starts impact ionisation and the growth of an electron avalanche. The space charge that forms strengthens the electric field that was already there. This causes the avalanche-to-streamer transition, where positive streamers quickly move towards the cathode, creating the dense and stable discharge current peaks seen in Figure 3 [32, 33]. During the negative half-cycle, on the other hand, electrons stick to oxygen molecules to make negative ions. At the same time, positive ions slowly move towards the high-voltage electrode, which only allows for micro-glow discharges of lower intensity and shorter duration [34].

At that point, looking at Figures 3(a–c), you can see that the micro-discharge current is much larger with the triangle voltage signal, which is more consistent and has a higher density. The triangle waveform's natural features make it possible for micro-discharge production to last up to 0.75 ms, which means that discharge can happen in practically every time interval of the

17518830, 2026, 1, Downloaded from https://ietresearch.onlinelibrary.wiley.com/doi/10.1049/smt2.70070 by Egyptian National Sti. Network (Enstinet), Wiley Online Library on [24/06/2026]. See the Terms and Conditions (https://onlinelibrary.wiley.com/terms-and-conditions) on Wiley Online Library for rules of use; OA articles are governed by the applicable Creative Commons License

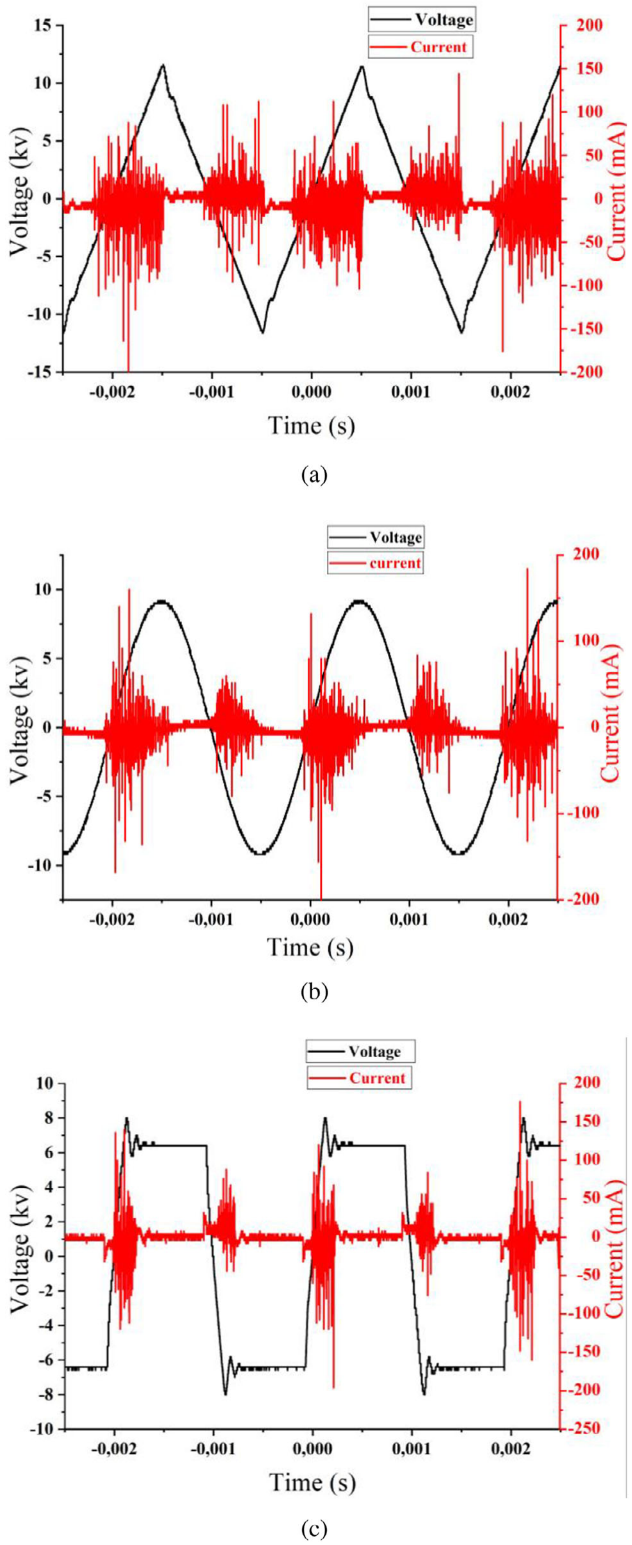

FIGURE 3 | Voltage and discharge current waveforms using: (a) Triangular, (b) Sinusoidal and (c) Rectangular signals.

signal. The sinusoidal signal provides a discharge current that is a little lower than the triangle waveform. This happens for 0.5 ms during the positive half-cycle. The rectangular waveform, on the other hand, has a much lower discharge density. Current only flows during voltage transitions for 0.25 ms, which shows that it doesn't work as well as the other waveforms.

There are two primary physical mechanisms responsible for the observed shift between the applied voltage peaks and the discharge current peaks. First, when the electric field in the discharge gap reaches the breakdown threshold—which is dependent on the gas composition, pressure, and gap geometry—micro-discharges are initiated. Sharp current peaks are produced when short-lived micro-discharges break down. The accumulated surface charges then quickly lower the local electric field, putting an end to the discharge before the voltage reaches its maximum value. Second, the phase shift between voltage and current peaks is further influenced by the accumulation and diffusion of charges on the dielectric surface, which alter the local electric field regardless of the instantaneous applied voltage [35, 36].

Lissajous figures for all voltage waveforms used are illustrated in Figure 4 at $V = 7.5$ kV. Equation 2 was used to calculate the consumed energy in these examples. The sinusoidal signal consumed the least energy at 65.85 W, while the triangular pulse wave consumption was the highest at 80.19 W, and by contrast, the rectangular waveform exhibited minimal discharge currents but maximal energy consumption with a value of 90.11 W. A repaired current deficiency observation provokes interesting questions about the possible relationship between discharged current and energy cost, especially for rectangular waveforms. If you want to operate SDBD-type reactors in real life, you need to know how these dynamics play out.

4.2 | Ozone Production

Applied voltage V, operating frequency F and voltage waveform shape were studied with regard to the efficiency of ozone in a DBD reactor. We then analysed three waveforms – the triangular, rectangular and sinusoidal forms – to determine their effects on ozone generation and energy utilisation.

One factor at a time (OFAT) was employed, and the ranges of voltage and frequency were selected so that each factor could be examined independently. The measurement was done twice for every experimental condition. Only when the difference between the two measurements was less than 5% were the results deemed valid. To guarantee reliability, a third measurement was carried out in situations where this threshold was exceeded. This method, which maintains a respectable number of experiments while offering a sufficient degree of reproducibility, is extensively used in the experimental DBD literature.

Experiment 1: The applied voltage (3–9 kV) was varied at a fixed frequency of 500 Hz.

Experiment 2: The frequency was varied from 100 to 1000 Hz, with an applied voltage of 7.5 kV.

Results from these experiments are shown in Figures 5 and 6 that illustrate how the three adjustable operating parameters impact ozone production (mg/L) and energy efficiency (g/kWh). In these charts, the impact of each control unit on the system performance measures becomes very evident.

Figure 5 shows that there is a clear and direct link between the voltage applied and the ozone concentration (Co_3) that results.

17518830, 2026, 1, Downloaded from https://ietresearch.onlinelibrary.wiley.com/doi/10.1049/smt2.70070 by Egyptian National Sti. Network (Enstinet), Wiley Online Library on [24/06/2026]. See the Terms and Conditions (https://onlinelibrary.wiley.com/terms-and-conditions) on Wiley Online Library for rules of use; OA articles are governed by the applicable Creative Commons License

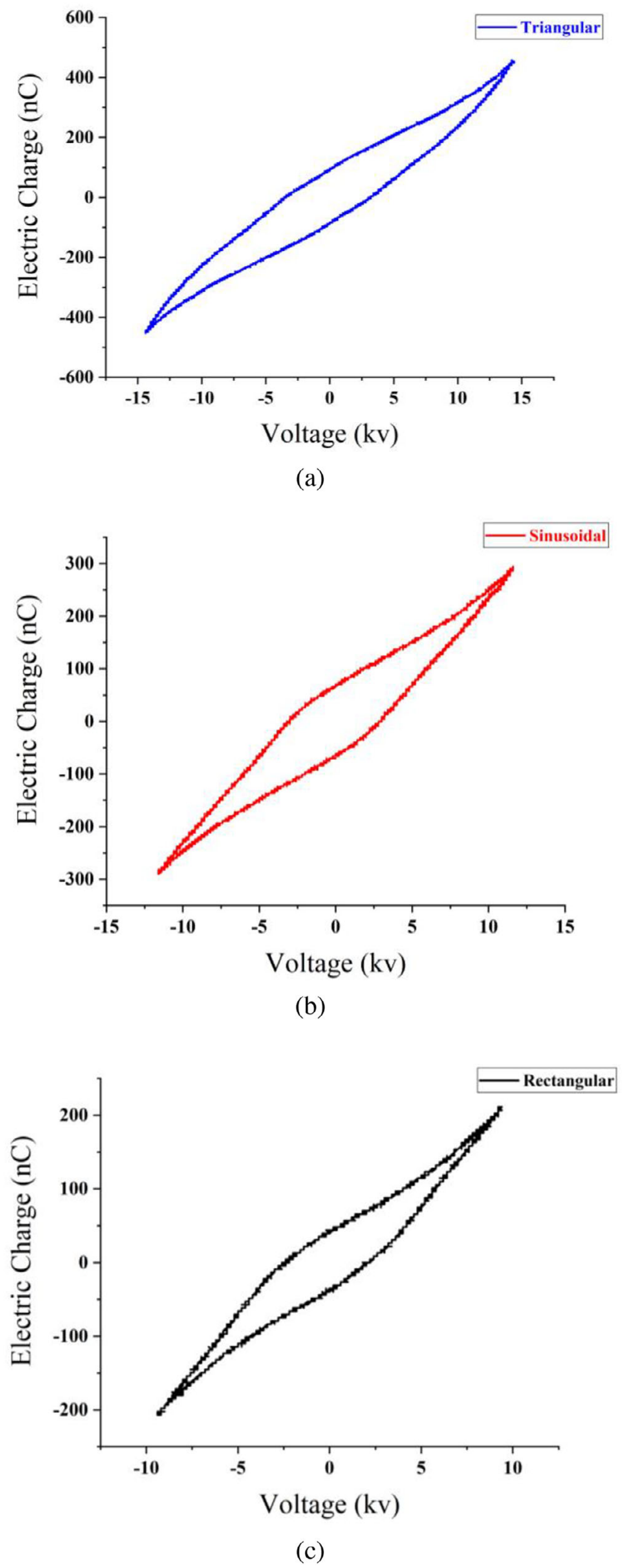

FIGURE 4 | Lissajous figures obtained for the three voltage waveforms (V_{rms} = 7.5 kV,500 Hz); (a) Triangular, (b) Sinusoidal and (c) Rectangular signals.

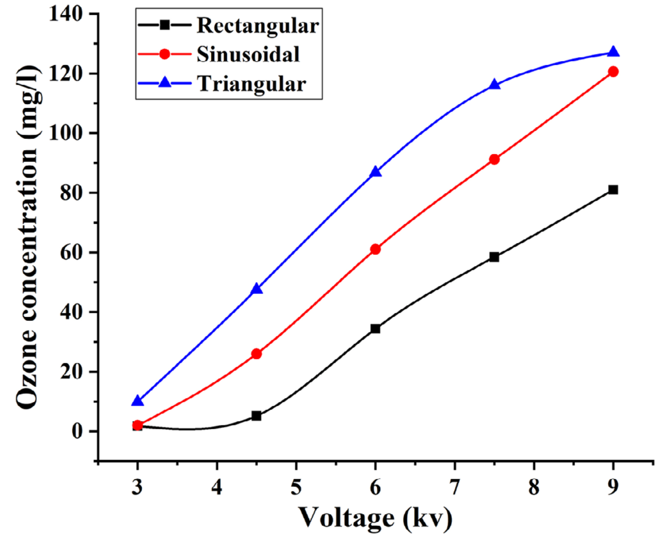

FIGURE 5 | Ozone production rate according to the voltage for the three voltage waveforms (500 Hz).

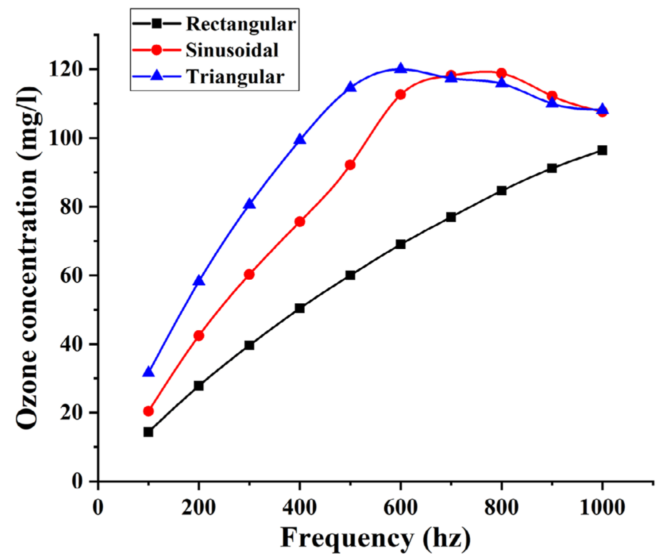

FIGURE 6 | Ozone production rate according to the frequency for the three voltage waveforms (7.5 kV).

The statistics clearly show that raising the applied voltage leads to higher levels of ozone concentration. This is because the dielectric barrier discharge (DBD) process is more active. This happens because higher voltage levels provide free electrons in the discharge zone more kinetic energy. This higher electron energy increases the collision cross-section between energetic electrons and gas molecules, which makes both the ionisation and dissociation processes that are necessary for ozone production stronger. This leads to more micro-discharges. However, too high voltages can lose energy because they cause the gas and dielectric barrier to heat up more, which wastes energy and lowers the overall process efficiency [37–39].

The triangular waveform was the best because it started both discharge and ozone production at a voltage as low as 3 kV, making the ozone concentration about 10 mg/L. The sinusoidal waveform needed 4.5 kV, and the rectangular waveform needed 6

17518830, 2026, 1, Downloaded from https://ietresearch.onlinelibrary.wiley.com/doi/10.1049/smt2.70070 by Egyptian National Sti. Network (Enstinet), Wiley Online Library on [24/06/2026]. See the Terms and Conditions (https://onlinelibrary.wiley.com/terms-and-conditions) on Wiley Online Library for rules of use; OA articles are governed by the applicable Creative Commons License

TABLE 1 | Discharge Inception Voltage and Ozone Generation Inception Voltage (10 mg/L) for each voltage waveform.

Waveform	Discharge Inception Voltage	Ozone Generation Inception Voltage (for 10 mg/l)
Triangular	2.5 kV	3 kV
Sinusoidal	3 kV	4 kV
Rectangular	4.5 kV	5.5 kV

kV to make the same amount of ozone that could be detected. It is important to note that the start of ozone production does not always happen at the same time as the start of electrical discharge. This is because early discharge activity can happen at lower voltages without making ozone effectively. Only when the discharge has enough intensity and density does ozone start to form. The triangular waveform has a higher discharge intensity and density than the sinusoidal and rectangular waveforms, which is why the inception voltage is different. Table 1 shows the discharge inception voltage and the ozone generation inception voltage for each waveform.

Figure 6 shows a similar pattern in the levels and frequency of ozone. When the applied voltage frequency went up, the ozone concentration went up a lot. This is because higher frequencies make micro-discharge events happen more often in the DBD reactor. When ions oscillate at greater frequencies, they hit each other more often and make more oxygen atoms available. This improves the production of ozone and the efficiency of energy use [40]. The triangle waveform consistently produced more ozone than the other waveforms in much of the frequency range, with the highest concentrations occurring around 120 mg/L around 600 Hz. The rectangular waveform, on the other hand, produced much less ozone, with a maximum of only 96 mg/L at 1000 Hz.

4.3 | Energy Efficiency

Figures 7 and 8 show how energy efficiency changes with voltage and frequency, respectively. The triangle voltage waveform outperformed the other waveforms in both ozone production and energy efficiency. The triangular waveform had a maximum energy efficiency of about 100 g/kWh at an applied voltage of about 4.5 kV. This was better than the sinusoidal waveform, which had a maximum of 86 g/kWh at 6.5 kV, and the rectangular waveform, which only had a maximum of 60 g/kWh at 9 kV.

Also, the triangular voltage waveform was more energy-efficient than the square wave across the whole frequency range of 0 to 1000 Hz. At 200 Hz, the triangle waveform had the highest energy efficiency of 120 g/kWh. This is far greater than the rectangular waveform's highest of 65 g/kWh and the sinusoidal waveform's highest of 95 g/kWh in their best frequency ranges.

The energy efficiency of the rectangular voltage waveform in Figure 7 followed a different pattern than the sinusoidal and triangular waveforms. The rectangular waveform's lower discharge generation caused energy efficiency to drop from 100 to 300 Hz. To make effective ozone, higher frequencies were needed.

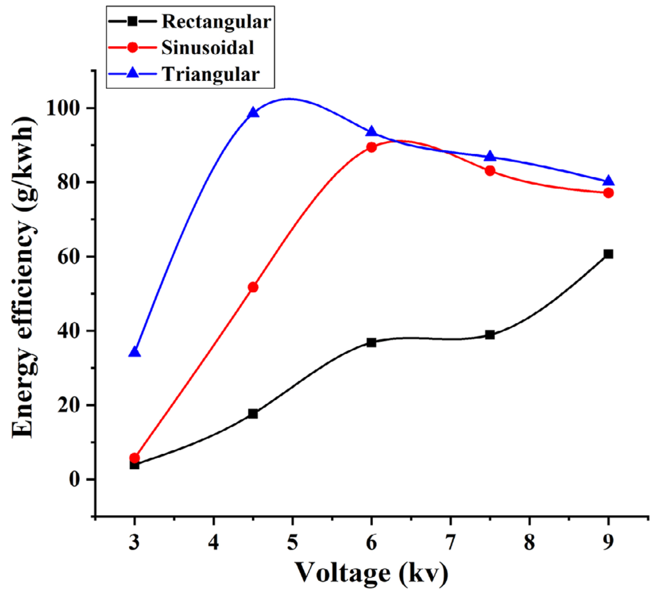

FIGURE 7 | Energy efficiency according to the voltage for the three voltage waveforms (500 Hz).

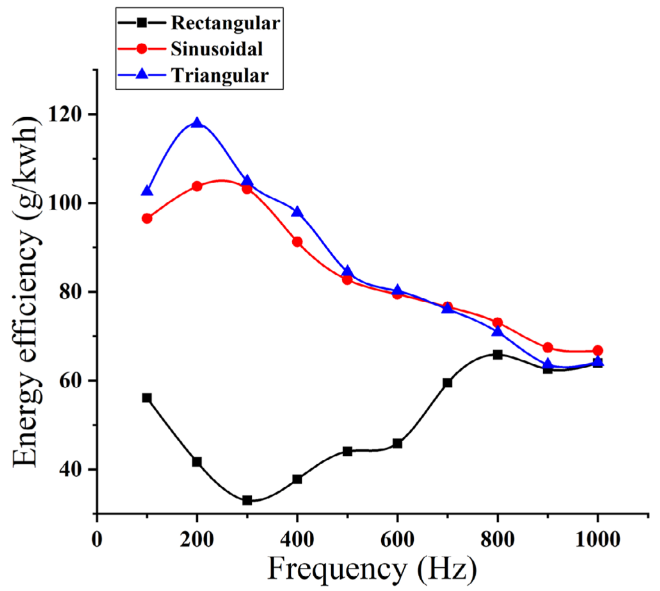

FIGURE 8 | Energy efficiency according to the frequency for the three voltage waveforms (7.5 kV).

Equation 3 shows that this higher energy use and reduced ozone production led to lower energy efficiency. When the frequency reached the best level of 400 Hz, when fairly intense discharges were generated, the energy efficiency went up a lot and stayed stable at 1000 Hz since the ozone production went up a lot.

In general, the triangular waveform is the most energy-efficient choice. This suggests that it might be used to improve the way ozone is made in real-world situations.

Although the triangular voltage waveform demonstrated superior performance under both voltage and frequency variations, the proper selection of these operating parameters remains essential. Consequently, the operational ranges for the applied voltage

17518830, 2026, 1, Downloaded from https://ietresearch.onlinelibrary.wiley.com/doi/10.1049/smt2.70070 by Egyptian National Sti. Network (Enstinet), Wiley Online Library on [24/06/2026]. See the Terms and Conditions (https://onlinelibrary.wiley.com/terms-and-conditions) on Wiley Online Library for rules of use; OA articles are governed by the applicable Creative Commons License

TABLE 2 | Final results of CCF design experiment.

Exp.	Voltage V (KV)	Frequency F (Hz)	Ozone concentration (mg/l)	Energy efficiency (g/kWh)
1	9	100	40.8	116.949
2	3	1000	19.4	30.069
3	9	1000	125.373	53.4655
4	3	550	10.4	29.931
5	9	550	124,4	73,121
6	6	100	20	102.418
7	6	1000	104.2	64.254
8	6	550	88	86.642
9	6	550	88	86.642
10	6	550	88	86.624

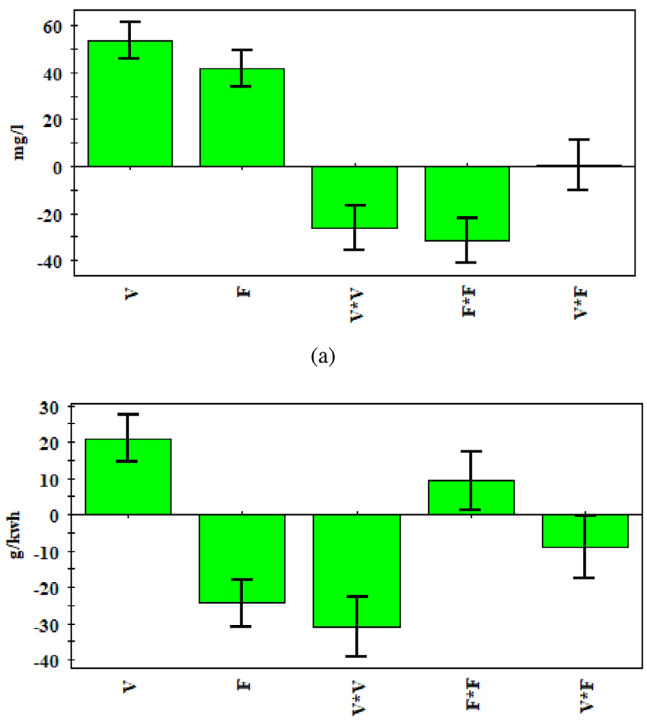

FIGURE 9 | Plotted coefficients of the obtained models for (a) ozone concentration CO_3 (mg/l) and (b) energy efficiency N (g/kWh).

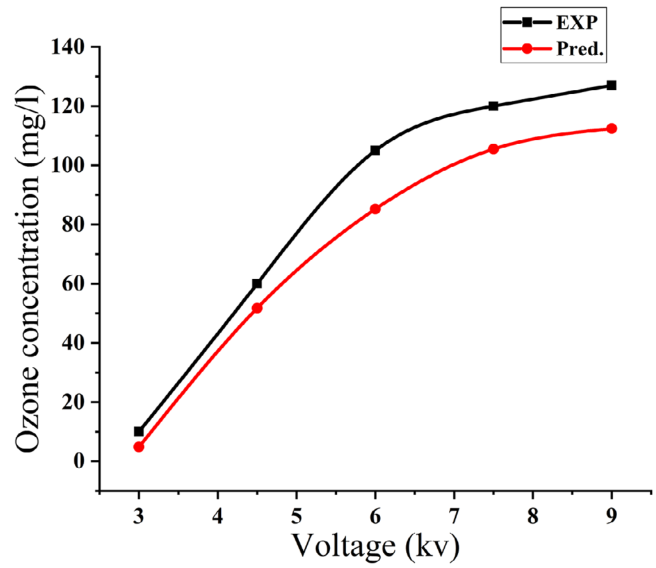

FIGURE 10 | Comparison between experimental and predicted ozone concentration (CO_3) as a function of applied voltage for the triangular waveform (F = 500 Hz).

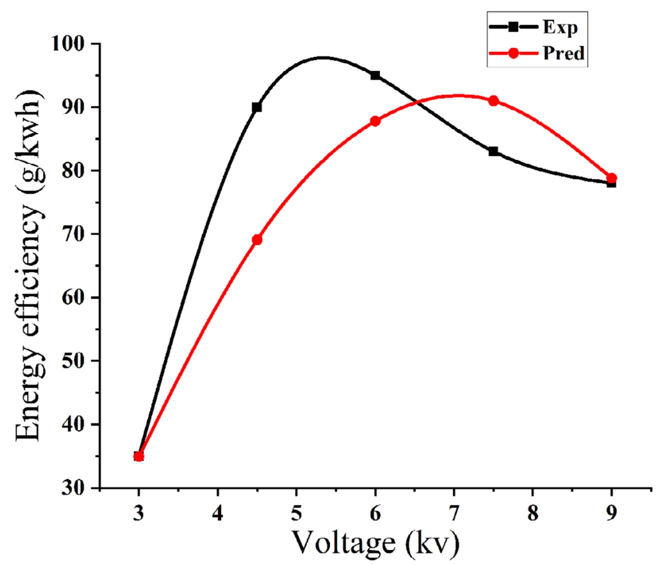

FIGURE 11 | Comparison between experimental and predicted energy efficiency (N) as a function of applied voltage for the triangular waveform ($F = 500$ Hz).

(V) and frequency (F) parameters were established based on the experimental findings and observations obtained during this preliminary investigation phase.

- $V_{max} = 9$ kV; $V_{min} = 3$ kV
- $F_{max} = 1000$ Hz; $F_{min} = 100$ Hz

4.4 | Set Point Identification

It is important to note that the operating ranges (V_{min}, V_{max}) and (F_{min}, F_{max}) were determined from preliminary one-factor-at-a-time (OFAT) experiments, presented in Figures 5–8. These OFAT experiments were conducted solely to identify the regions where the system responds significantly and to avoid areas of low performance or instability. Subsequently, a completely independent Composite Centred Faces (CCF) design was executed, in which voltage and frequency were varied simultaneously according to a structured matrix (factorial points, centre points and axial points). The results of this CCF design are presented in Table 2, and were used to construct the mathematical models and response surfaces presented in this section.

A central CCF design was used to get the ideal values for both components. The restrictions set in the previous section for each

17518830, 2026, 1, Downloaded from https://ietresearch.onlinelibrary.wiley.com/doi/10.1049/smt2.70070 by Egyptian National Sti. Network (Enstinet), Wiley Online Library on [24/06/2026]. See the Terms and Conditions (https://onlinelibrary.wiley.com/terms-and-conditions) on Wiley Online Library for rules of use; OA articles are governed by the applicable Creative Commons License

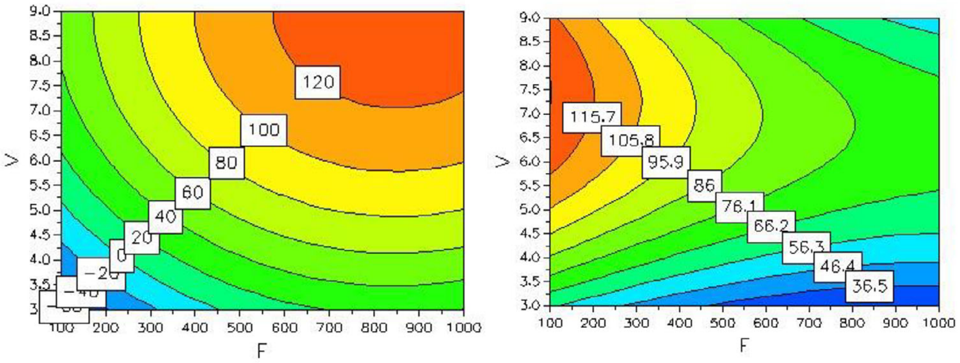

(a) Ozone concentration CO3 (mg/l) (b) energy efficiency N (g/kWh)

FIGURE 12 | Voltage-frequency response contour plots for (a) Ozone concentration and (b) Energy efficiency.

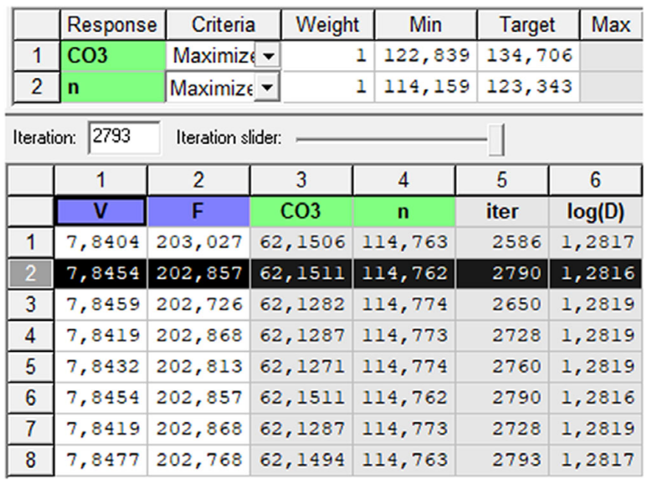

	Response	Criteria	Weight	Min	Target	Max
1	CO3	Maximize	1	122,839	134,706	
2	n	Maximize	1	114,159	123,343	

Iteration: 2793 Iteration slider:

	1	2	3	4	5	6
	V	F	CO3	n	iter	log(D)
1	7,8404	203,027	62,1506	114,763	2586	1,2817
2	7,8454	202,857	62,1511	114,762	2790	1,2816
3	7,8459	202,726	62,1282	114,774	2650	1,2819
4	7,8419	202,868	62,1287	114,773	2728	1,2819
5	7,8432	202,813	62,1271	114,774	2760	1,2819
6	7,8454	202,857	62,1511	114,762	2790	1,2816
7	7,8419	202,868	62,1287	114,773	2728	1,2819
8	7,8477	202,768	62,1494	114,763	2793	1,2817

FIGURE 13 | The outcomes of the optimisation process in MODDE 5.0 are a maximum of both ozone concentration and energy efficiency.

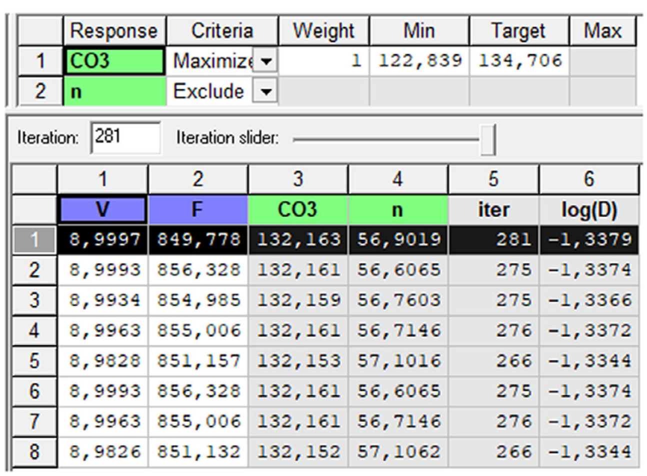

	Response	Criteria	Weight	Min	Target	Max
1	CO3	Maximize	1	122,839	134,706	
2	n	Exclude				

Iteration: 281 Iteration slider:

	1	2	3	4	5	6
	V	F	CO3	n	iter	log(D)
1	8,9997	849,778	132,163	56,9019	281	-1,3379
2	8,9993	856,328	132,161	56,6065	275	-1,3374
3	8,9934	854,985	132,159	56,7603	275	-1,3366
4	8,9963	855,006	132,161	56,7146	276	-1,3372
5	8,9828	851,157	132,153	57,1016	266	-1,3344
6	8,9993	856,328	132,161	56,6065	275	-1,3374
7	8,9963	855,006	132,161	56,7146	276	-1,3372
8	8,9826	851,132	132,152	57,1062	266	-1,3344

FIGURE 14 | The outcomes of the optimisation process in MODDE 5.0 for maximum ozone concentration.

of the two variables ($V_{\min}$, $V_{\max}$) and ($F_{\min}$, $F_{\max}$) are represented by the two levels, 'max' and 'min'. The following formula was used to determine the central point (V_c, F_c):

$$V = (V_{min} + V_{max})/2 = \frac{3+9}{2} = 6 \text{ kV} \quad (8)$$

$$F = (F_{min} + F_{max})/2 = \frac{100+1000}{2} = 550 \text{ Hz} \quad (9)$$

The definitive outputs of the CCF design experiment are shown in Table 2. Table 2 shows the energy efficiency (g/kWh) and ozone concentration (g/h), which were taken to be meaningful responses.

The mathematical models proposed by MODDE 5.0 are as follows:

$$\text{CO3 (mg/L)} = 90.27 + 53.90 \cdot V + 41.80 \cdot F - 26.65 \cdot V^2 - 31.57 \cdot F^2 + 0.64 \cdot V \cdot F$$

$$\text{N (g/kWh)} = 84.98 + 20.93 \cdot V - 24.42 \cdot F - 30.96 \cdot V^2 + 9.35 \cdot F^2 - 8.90 \cdot V \cdot F$$

Where V and F are the scaled and centred values of the applied voltage and frequency, respectively.

We used MODDE 5.0 to get the mathematical model for CO_3 (mg/l) and n (g/kWh) and plot it as shown in Figure 9. We checked the model's validity using two statistical tests: the coefficient of determination R^2 and the cross-validated coefficient of prediction Q^2. The values of $R^2 = 0.994$ and $Q^2 = 0.915$ for the response to ozone concentration, and $R^2 = 0.992$ and $Q^2 = 0.875$ for the response to energy efficiency, show that the model fits well and can make good predictions. Also, the difference between R^2 and Q^2 is less than 0.2 in both cases, which is what is needed for RSM model validation.

From the results depicted in Figure 9, it's evident that both factors V and F have a notable impact on both the ozone concentration (CO_3) in mg/l and the energy efficiency (N) in g/kWh. Furthermore, there appears to be no interaction effect between V and F in ozone concentration nor in energy efficiency associated with the voltage-squared and frequency effects. Consequently, optimisation should be done to determine the ideal values of both variables that yield the highest possible levels of energy efficiency and ozone concentration.

17518830, 2026, 1, Downloaded from https://ietresearch.onlinelibrary.wiley.com/doi/10.1049/smt2.70070 by Egyptian National Sti. Network (Enstinet), Wiley Online Library on [24/06/2026]. See the Terms and Conditions (https://onlinelibrary.wiley.com/terms-and-conditions) on Wiley Online Library for rules of use; OA articles are governed by the applicable Creative Commons License

To further support the validity of the proposed mathematical models, Figures 10 and 11 illustrate a comparison between the experimentally measured values and the model-predicted values for ozone concentration (CO_3) and energy efficiency (N), respectively, as a function of the applied voltage for the triangular waveform. Both figures demonstrate that the predicted values follow the same general trend as the experimental data across the entire voltage range. The model captures the characteristic behaviour of both responses: the monotonic increase in ozone concentration with voltage and the presence of an optimal voltage value for maximum energy efficiency. The observed deviations between experimental and predicted values remain within an acceptable range, consistent with the high R^2 and Q^2 values reported for both models ($R^2 = 0.994$, $Q^2 = 0.915$ for CO_3 and $R^2 = 0.992$, $Q^2 = 0.875$ for N). These results confirm the reliability and predictive capability of the RSM-based mathematical models developed in this study.

A graphical visualisation of the reaction is provided by the MODDE 5.0 software. The iso-response contours produced by the current mathematical model are shown in Figure 12(a) and Figure 12(b). These contours show curves that, when two factors are varied while the other variable remains constant, indicate a consistent reaction. Every contour on the response surface represents a certain level [41].

Finding the ideal settings for variables that provide the highest ozone concentration and energy efficiency is made easier by the software. It includes an optimisation process that can handle several replies modified by different weighting coefficients at the same time. Based on the two different answers, the optimiser tool searches for the optimal solution to an equation. The 'limit optimisation' analysis is the default approach in MODDE 5.0. In this case, the goal is to maximise both ozone concentration and energy efficiency by creating a solution where the response fits within predetermined bounds.

This model indicates that for V = 7.84 kV and f = 202.86 Hz, which gives us $n = 114.76$ g/kWh, process optimisation (the highest level of energy efficiency) is shown in Figure 13. The optimiser suggests a different set point, $V = 8.99$ kV, $F = 849.7$ Hz, which corresponds to OC = 132.163 mg/l if ozone formation is thought to be a more significant reaction than energy efficiency (Figure 14).

5 | Conclusion

This study evaluates the impact of different voltage waveforms – triangular, rectangular and sinusoidal – on ozone production and energy efficiency in surface dielectric barrier discharge (SDBD) reactors. The triangular waveform proved most effective, yielding a maximum ozone concentration of 132.163 mg/L and energy efficiency of 114.76 g/kWh under optimal conditions. In contrast, for the rectangular and sine waveforms, lower ozone productions were obtained, showing a proper choice of waveform is necessary to maximise reactor working in this type of reactor. Voltage and frequency increase ozone generation, but for higher values, energy efficiency decreases; thus, an optimum should be achieved. By using RSM, operating conditions were effectively modelled and optimised. The results of the study contribute to SDBD reactor development and indicate that further studies should be carried out on plasma discharge mechanisms associated with waveform effects, which could potentially improve reactors' performance and their industrial scalability.

Author Contributions

Brahim el Khalil Oulad Naoui, Said Nemmich, Kamel Nassour, Essama Ahmed Ghaitaoui and Amar Tilmatine: conceptualisation, methodology, software, visualisation, investigation, writing – original draft preparation. Sherif Salama Mohamed Ghoneim, Amanuel Kumsa Bojer, Sayed Ahmed Nagy, Ahmed Mohammed Attiya Soliman and Ahmed M. Hussein: data curation, validation, supervision, resources, writing – review and editing, project administration and funding acquisition.

Acknowledgements

The authors would like to acknowledge the Deanship of Graduate Studies and Scientific Research, Taif University, for funding this work.

Funding

This work is funded and supported by the Deanship of Graduate Studies and Scientific Research, Taif University.

Conflicts of Interest

The authors declare no conflicts of interest.

Data Availability Statement

The datasets used and/or analysed during the current study are available from the corresponding author on reasonable request.

References

1. K. Hussain, N. A. Khan, V. Vambol, S. Vambol, S. Yeremenko, and V. Sydorenko, "Advancement in Ozone Base Wastewater Treatment Technologies: Brief Review," *Ecological Questions* 33, no. 2 (February 2022): 1–23, https://doi.org/10.12775/EQ.2022.010.

2. L. Nehari, S. Nemmich, A. Tilmatine, and S. M. Remaoun, "Adaptation of a Photovoltaic Powered Ozone Generationsystem for Food Storage," *Carpathian Journal of Food Science and Technology* (December 2019): 64–71, https://doi.org/10.34302/2019.11.4.5.

3. A. Rizky, D. Tanjung, and K. Khairunnisa, "The Effect of Ozone Therapy Stimulation on Diabetes Wound Healing Process," *Contagion: Scientific Periodical Journal of Public Health and Coastal Health* 6, no. 1 (March 2024): 480, https://doi.org/10.30829/contagion.v6i1.19602.

4. H. M. Talebi, J. Javaheri, and M. S. Fakhari, "Successful Treatment of a High-Risk Diabetic Foot Ulcer by Ozone Therapy and Collagen Powder: A Case Report," *Clinical Case Reports* 12, no. 4 (April 2024): e8728, https://doi.org/10.1002/ccr3.8728.

5. C. Khosla, Mamta, and Anuradha, "Treatment of Dental Caries by Ozone Therapy—A Review," *Journal of Chemical and Environmental Sciences and Its Applications* 1, no. 1 (Sep. 2014): 15–22, https://doi.org/10.15415/jce.2014.11002.

6. M. Horvath, L. Bilitzky, and J. Huettner, "Production by Chemonuclear Methods," in *Ozone*, eds. M. Horvath, L. Bilitzky, and J. Huettner (Elsevier, 1985), 104–106, accessed March 2, 2024, https://inis.iaea.org/search/search.aspx?orig_q=RN.

7. K. Nassour, M. Brahami, S. Nemmich, N. Hammadi, A. Tilmatine, and N. Zouzou, "A New Hybrid Surface-Volume Dielectric Barrier Discharge Reactor for Ozone Generation," *IEEE Transactions on Industry Applications* 53, no. 3 (2017): 2477–2484.

8. A. Tilmatine, N. Hammadi, S. M. Remaoun, K. Medles, S. Nemmich, and L. Dascalescu, "Processes for Sustainable Development Using High-

17518830, 2026, 1, Downloaded from https://ietresearch.onlinelibrary.wiley.com/doi/10.1049/smt2.70070 by Egyptian National Sti. Network (Enstinet), Wiley Online Library on [24/06/2026]. See the Terms and Conditions (https://onlinelibrary.wiley.com/terms-and-conditions) on Wiley Online Library for rules of use; OA articles are governed by the applicable Creative Commons License

Intensity Electric Fields," *International Journal of Sustainable Engineering* 6, no. 2 (June 2013): 177–185, https://doi.org/10.1080/19397038.2012.665507.

9. E. Yulianto, R. S. Darmawan, S. Sumariyah, M. Nur, Z. Muchasin, and A. Wardane, "Comparison of Ozone Production by DBDP Reactors: Difference External Electrodes," *Journal of Physics: Conference Series, IOP Publishing* 1153, no. 1 (2019): 012088, https://doi.org/10.1088/1742-6596/1153/1/012088.

10. U. Kogelschatz, "Dielectric-Barrier Discharges: Their History, Teratogenesis, and Applications," *Plasma Chemistry and Plasma Processing* 23, no. 1 (2003): 1–46, https://doi.org/10.1023/A:1022470901385.

11. O. N. Brahim el Khalil, N. Said, N. Kamel, G. E. Ahmed, B. Yassine, and T. Amar, "Comparative Experimental Study of Voltage Waveform Influences on Ozone Production Efficiency," In *2024 3rd International Conference on Advanced Electrical Engineering (ICAEE)*, (IEEE, 2024), 1–6, https://doi.org/10.1109/ICAEE61760.2024.10783232.

12. M. Štefečka, D. Korzec, M. Širý, Y. Imahori, and M. Kando, "Experimental Study of Atmospheric Pressure Surface Discharge in Helium," *Science and Technology of Advanced Materials* 2 (September 2001): 587, https://doi.org/10.1016/S1468-6996(01)00141-3.

13. S. Pekárek, "Experimental Study of Surface Dielectric Barrier Discharge in Air and Its Ozone Production," *Journal of Physics D: Applied Physics* 45 (February 2012): 075201, https://doi.org/10.1088/0022-3727/45/7/075201.

14. S. Xie, Y. He, D. Yuan, and Z. Luo, "The Effects of Gas Flow Pattern on the Generation of Ozone in Surface Dielectric Barrier Discharge," *Plasma Science and Technology* 21, no. 5 (May 2019): 055505, https://doi.org/10.1088/2058-6272/aafc50.

15. S. Nemmich, M. Elmouloud Zelmat, K. Nassour, N. Hammadi, A. Draou, and A. Tilmatine, "Experimental Analysis of the Influence of the Voltage Waveform on Ozone Generation Efficiency," *International Journal of Environmental Studies* 76, no. 4 (July 2019): 571–581, https://doi.org/10.1080/00207233.2019.1594411.

16. B. Choudhury, S. Portugal, S. Roy, E. Mastro, and J. A. Johnson, "Smart Dielectric Barrier Discharge Plasma Decontamination: Spatially Targeted Decontamination With Actuated Ozone Distribution," *Frontiers in Physics* 10 (March 2022): 834030, https://doi.org/10.3389/fphy.2022.834030.

17. N. Mericam-Bourdet, M. J. Kirkpatrick, F. Tuvache, D. Frochot, and E. Odic, "Effect of Voltage Waveform on Dielectric Barrier Discharge Ozone Production Efficiency," *European Physical Journal Applied Physics* 57, no. 3 (March 2012): 30801, https://doi.org/10.1051/epjap/2012110302.

18. G. Huang, Y. Zhou, T. Wang, S. Zhang, and J. Li, "Statistical Analysis of Pulsed Microdischarges and Ozone Generation in Dielectric Barrier Discharges," *IEEE Transactions on Plasma Science* 44, no. 10 (October 2016): 2111–2120, https://doi.org/10.1109/TPS.2016.2570758.

19. S. Nemmich, K. Nassour, M. N. Brahami, and N. Hammadi, N. Zouzou, and A. Tilmatine, "Development and Optimization of an Ozone Food preservation System Using Response Surface Modelling (RSM)," *Carpathian Journal of Food Science and Technology* 13, no. 4 (2021): 35–46, https://doi.org/10.34302/crpjfst/2021.13.4.4.

20. A. Draou, S. Nemmich, K. Nassour, Y. Benmimoun, and A. Tilmatine, "Experimental Analysis of a Novel Ozone Generator Configuration for Use in Water Treatment Applications," *International Journal of Environmental Studies* 76, no. 2 (March 2019): 338–350, https://doi.org/10.1080/00207233.2018.1499698.

21. B. E. K. Oulad Naoui, S. Nemmich, K. Nassour, M. N. Brahami, B. N. Dahane, and A. Tilmatine, "A Novel Double-Gap Dielectric Barrier Discharge (DG-DBD) for Enhanced Ozone Generation," *Vacuum* 246 (January 2026): 115071, https://doi.org/10.1016/j.vacuum.2026.115071.

22. K. Nassour, M. Brahami, A. Tilmatine, N. Zouzou, and L. Dascalescu, "Comparative Experimental Analysis of Ozone Generation Between Surface and Volume DBD Generators," *IEEE Transactions on Dielectrics and Electrical Insulation* 25, no. 2 (April 2018): 428–434, https://doi.org/10.1109/TDEI.2017.006600.

23. N. L. Frigon and D. Mathews, *Practical Guide to Experimental Design*. (John Wiley & Sons, 1996), https://books.google.com/books?id=xV_WhIcPMrEC.

24. L. Eriksson, E. Johansson, N. Kettaneh-Wold, C. Wikström, and S. Wold, *Design of Experiments: Principles and Applications*. (Stockholm, 2000).

25. E. Khelifi, M. N. Brahami, I. S. Bousmaha, et al., "Optimization of Ozone Generator Sizing and Performance Using Response Surface Modeling and Metaheuristic Algorithms: A Comparative Study of HLOA and LCA," *Journal of the Korean Physical Society* 86 (March 2025): 856–874, https://doi.org/10.1007/s40042-025-01302-z.

26. G. E. Ahmed, N. Kamel, N. Said, B. E. K. Oulad Naoui, Y. Benmimoun, and A. Tilmatine, "Optimization of Water Treatment Process With Ozone Generated by DBD Using PSO Algorithm," in 2023 second international conference on energy transition and security (ICETS), (IEEE, 2023), 1–5, https://doi.org/10.1109/ICETS60996.2023.10410775.

27. M. T. Layati, K. Nassour, S. Nemmich, M. Brahami, and A. Tilmatine, "Experimental Analysis of a Cylindrical Ozone Generator With a Partitioned High-Voltage Electrode," *Ozone Science and Engineering* 43, no. 4 (July 2021): 339–350, https://doi.org/10.1080/01919512.2020.1812376.

28. E. A. Ghaitaoui, K. Nassour, S. Nemmich, et al., "Experimental Comparative Study Between Simple and Multi-Tube DBD Ozone Generator With Same Volume Discharge for Wastewater Treatment," *Journal of the Korean Physical Society* 85 (September 2024): 1–12, https://doi.org/10.1007/s40042-024-01179-4.

29. K. Takaki, M. Shimizu, S. Mukaigawa, and T. Fujiwara, "Effect of Electrode Shape in Dielectric Barrier Discharge Plasma Reactor for NOx Removal," *IEEE Transactions on Plasma Science* 32, no. 1 (February 2004): 32–38, https://doi.org/10.1109/TPS.2004.823973.

30. M. Tański, A. Reza, D. Przytuła, and K. Garasz, "Ozone Generation by Surface Dielectric Barrier Discharge," *Applied Sciences* 13, no. 12 (June 2023): 7001, https://doi.org/10.3390/app13127001.

31. Y. Jiang, B. Peng, Z. Liu, H. Xu, S. Zhang, and J. Li, "Characteristic Studies on Positive and Negative Streamers of Double-Sided Pulsed Surface Dielectric Barrier Discharge," *Plasma Science and Technology* 24, no. 4 (April 2022): 044005, https://doi.org/10.1088/2058-6272/ac58ed.

32. A. Chirokov, A. Gutsol, and A. Fridman, "Atmospheric Pressure Plasma of Dielectric Barrier Discharges," *Pure and Applied Chemistry* 77, no. 2 (2005): 487–495.

33. H. Wedaa, M. Abdel-salam, A. Ahmed, and A. Mizuno, "Two-Dimensional Modelling of Dielectric Barrier Discharges Using Charge Simulation Technique-Theory Against Experiment," *IET Science, Measurement and Technology* 8, no. 5 (2014): 285–293, https://doi.org/10.1049/iet-smt.2013.0147.

34. Z. Salam, M. Facta, M. Amjad, and Z. Buntat, "Design and Implementation of a Low Cost, High Yield Dielectric Barrier Discharge Ozone Generator Based on the Single Switch Resonant Converter," *IET Power Electronics* 6, no. 8 (2013): 1583–1591, https://doi.org/10.1049/iet-pel.2012.0470.

35. H. T. Truong, Y. Uesugi, and X. B. Nguyen, "Mechanisms of Low-Frequency Dielectric Barrier Discharge (DBD) Plasma Driven by Unipolar Pulses and Bipolar Pulses," *AIP Advances* 11, no. 2 (February 2021): 025022, https://doi.org/10.1063/5.0033846.

36. U. Kogelschatz, "Fundamentals and Applications of Dielectric-Barrier Discharges," In HAKONE VII Int. Symp. On High Pressure Low Temperature Plasma Chemistry, Greifswald 2000.

37. S. Li, X. Dang, X. Yu, G. Abbas, Q. Zhang, and L. Cao, "The Application of Dielectric Barrier Discharge Non-Thermal Plasma in VOCs Abatement: A Review," *Chemical Engineering Journal* 388 (May 2020): 124275, https://doi.org/10.1016/j.cej.2020.124275.

17518830, 2026, 1, Downloaded from https://ietresearch.onlinelibrary.wiley.com/doi/10.1049/smt2.70070 by Egyptian National Sti. Network (Enstinet), Wiley Online Library on [24/06/2026]. See the Terms and Conditions (https://onlinelibrary.wiley.com/terms-and-conditions) on Wiley Online Library for rules of use; OA articles are governed by the applicable Creative Commons License

38. T. Chang, Z. Shen, Y. Huang, et al., "Post-plasma-catalytic Removal of Toluene Using MnO_2–Co_3O_4 Catalysts and Their Synergistic Mechanism," *Chemical Engineering Journal* 348 (September 2018): 15–25, https://doi.org/10.1016/j.cej.2018.04.186.

39. T. Zhu, Y. D. Wan, J. Li, L. L. Wu, J. B. Ni, and J. Y. Sun, "Volatile Organic Compounds Decomposition Using Nonthermal Plasma Coupled With a Combination of Catalysts," *International Journal of Environmental Science and Technology* 8, no. 3 (June 2011): 621–630, https://doi.org/10.1007/BF03326247.

40. C. Subrahmanyam, M. Magureanu, A. Renken, and L. Kiwi-Minsker, "Catalytic Abatement of Volatile Organic Compounds Assisted by Non-Thermal Plasma," *Applied Catalysis B: Environmental* 65, no. 1–2 (May 2006): 150–156, https://doi.org/10.1016/j.apcatb.2006.01.006.

41. S. Bechekir, M. Brahami, D. J. O. Abdeslam, S. Nemmich, K. Nassour, and A. Tilmatine, "Development of a Low-Cost Ozone Generator Supply: Optimization Using Response Surface Modeling," *International Journal of Plasma Environmental Science and Technology* 13, no. 1 (2019): 7–13.

17518830, 2026, 1, Downloaded from https://ietresearch.onlinelibrary.wiley.com/doi/10.1049/smt2.70070 by Egyptian National Sti. Network (Enstinet), Wiley Online Library on [24/06/2026]. See the Terms and Conditions (https://onlinelibrary.wiley.com/terms-and-conditions) on Wiley Online Library for rules of use; OA articles are governed by the applicable Creative Commons License